18

Nanoelectrodes Integrated in Atomic Force Microscopy Cantilevers for Imaging of *In Situ* Enzyme Activity

Angelika Kueng, Christine Kranz, Alois Lugstein, Emmerich Bertagnolli, and Boris Mizaikoff

Summary

For investigation of laterally resolved information on biological activity, techniques for simultaneously obtaining complementary information correlated in time and space are required. In this context, recent developments in scanning probe microscopy are aimed at information on the sample topography and simultaneously on the physical and chemical properties at the nanometer scale. With the integration of submicro- and nanoelectrodes into atomic force microscopy (AFM) probes using microfabrication techniques, an elegant approach combining scanning electrochemical microscopy with AFM is demonstrated. This instrumentation enables simultaneous imaging of topography and obtainment of laterally resolved electrochemical information in AFM tapping mode. Hence, topographical and electrochemical information on soft surfaces (e.g., biological species) and polymers can be obtained. The functionality of tip-integrated electrodes is demonstrated by simultaneous electrochemical and topographical studies of an enzyme-modified micropattern.

Key Words: Scanning electrochemical microscopy; atomic force microscopy; enzyme activity; tapping mode; bifunctional scanning probe tips.

1. Introduction

Recent developments in the combination of scanning probe techniques are aimed at complementary, simultaneously obtained information about physical and chemical surface properties with high spatial resolution. Because many biochemically relevant processes are based on redox chemistry and electrochemical conversion of molecules, techniques gathering laterally resolved information on coupled oxidation-reduction processes are of particular interest. The combination of atomic force microscopy (AFM) ***(1)*** with scanning

From: *Methods in Molecular Biology, vol. 300:*
Protein Nanotechnology, Protocols, Instrumentation, and Applications
Edited by: T. Vo-Dinh © Humana Press Inc., Totowa, NJ

electrochemical microscopy (SECM) ***(2–4)*** is a particularly attractive strategy for achieving complementary electrochemical and topographical information with high lateral resolution in a single time- and space-correlated measurement ***(5)***. Microfabrication including focused ion beam (FIB) technology of submicro- and nanoelectrodes integrated into conventional AFM tips is an elegant and versatile approach combining SECM and AFM ***(6,7)***. The terms AFM and SECM are used for the instrument as well as the technique. An electroactive area is integrated at an exactly defined distance above the apex of the AFM tip ***(8)***, enabling contact mode and tapping mode operation ***(9)***. Application of AFM tapping mode ***(10)*** is a prerequisite for successfully imaging soft biological samples or polymers ***(11–13)***.

To illustrate the functionality and capability of this method, bifunctional probes with integrated electrodes are applied to simultaneously image topographical and electrochemical properties of a biologically active sample in AFM tapping mode. As an example, the activity of the oxidoreductase glucose oxidase immobilized at a periodic micropattern of a soft polymer matrix is electrochemically imaged during mapping of the topography ***(14)***. This concept is currently extended to AFM tip–integrated electrochemical biosensors for biomedical applications ***(15–17)***.

2. Materials

1. Atomic force microscope equipped with a tapping mode liquid cell (e.g., Nanoscope III; Digital Instruments, Santa Barbara, CA).
2. Bipotentiostat (Model 832A, CH-Instrument, Austin, TX).
3. FIB system.
4. DC-sputterer equipped with a Ti target.
5. RF-sputterer equipped with an Au or Pt target.
6. Vapor deposition polymerization (VDP) system or plasma-enhanced chemical vapor deposition (PECVD).
7. Silicon nitride AFM cantilevers with a length of 200 µm, an integrated pyramidal tip (base: 4×4 µm; height: 2.86 µm), and a spring constant of approx 0.06 Nm^{-1}.
8. Micropatterned gold/silicon nitride sample (Quantifoil, Jena, Germany).
9. Chloro-*p*-xylylene (parylene C).
10. Pt wire (diameter: 1 mm) as counterelectrode.
11. Ag/AgCl reference electrode or oxidized Ag wire (diameter: 1 mm) serving as a quasireference electrode (AgQRef).
12. Insulating varnish (RS Components, Northants UK).
13. Glucose oxidase (150,000 U/g, solid, from *Aspergillus niger*); store at –20°C.
14. Potassium ferrocyanide.
15. Potassium chloride.
16. 0.1 *M* Phosphate buffer (pH 7.0); store at 4°C.
17. Glucose.
18. EDP, Elektrodepositionslack Glassophor ZQ 8-43225, Canguard (BASF Farben und Lacke, Münster, Germany).

3. Methods

3.1. Preparation of AFM-SECM Tip

The steps described in **Subheadings 3.1.1.–3.1.3.** outline the procedure for preparation of the AFM-SECM tip including the metallization and insulation of the cantilever, the FIB cutting process to expose the electroactive area, and the characterization of the tip-integrated electrodes.

3.1.1. Metallization and Insulation of AFM Cantilevers

The silicon nitride AFM cantilevers were DC sputtered (CVC Products) with a 3-nm Ti adhesion layer (working pressure: 6 mtorr; power: 350 W; under argon). Subsequently, a 100-nm uniform gold layer was deposited using an RF-sputterer (working pressure: 6 mtorr; power: 150 W; under argon) to minimize mechanical stress on the cantilevers (*see* **Note 1**). To insulate the gold-coated cantilever, 700 nm of parylene C was deposited by VDP (*see* **Note 2**) ***(18)***. The polymerization process includes the following steps:

1. Initial vaporization at 150°C, 1.0 torr.
2. Cleaving into monomeric radicals by pyrolysis at 680°C, 0.5 torr.
3. Adsorption of the monomeric radical onto the sample (cantilever) surface and simultaneous polymerization.

3.1.2. FIB Milling of AFM-SECM Cantilevers

Figure 1 schematically illustrates the fabrication steps of an integrated frame microelectrode along with the FIB images of the milling processes. All modifications were carried out in a two-lens FIB system (Micrion 2500) utilizing a beam of Ga^+ ions at 50 keV.

Figure 1A shows the cantilever after coating with the metal layer and the insulation layer. The first FIB-milling step, diametrically opposed cuttings, as illustrated in **Fig. 1B**, determines the size of the integrated microelectrode. The same cutting procedure was repeated in a second step at the frontal areas of the pyramidal tip after a 90° turn of the cantilever (**Fig. 1C**). The following milling step (**Fig. 1D**) comprises reshaping the AFM tip and adjusting its length in correlation with the integrated electrode area. For optimum current responses according to SECM theory ***(19)***, the reshaped AFM tip (tip-substrate separation) should be $<0.7 \times$ electrode edge length (**Fig. 1F**). This milling step must be repeated again at the side and the frontal areas of the pillar to reshape the nonconducting original AFM tip. **Figure 1E** shows the integrated microelectrode after a final single-pass milling step to remove accumulated material resulting from previous cutting steps from the electroactive surface. Because of the reshaped AFM tip, this procedure ensures high resolution in topography and a precisely defined and constant distance between the integrated electrode

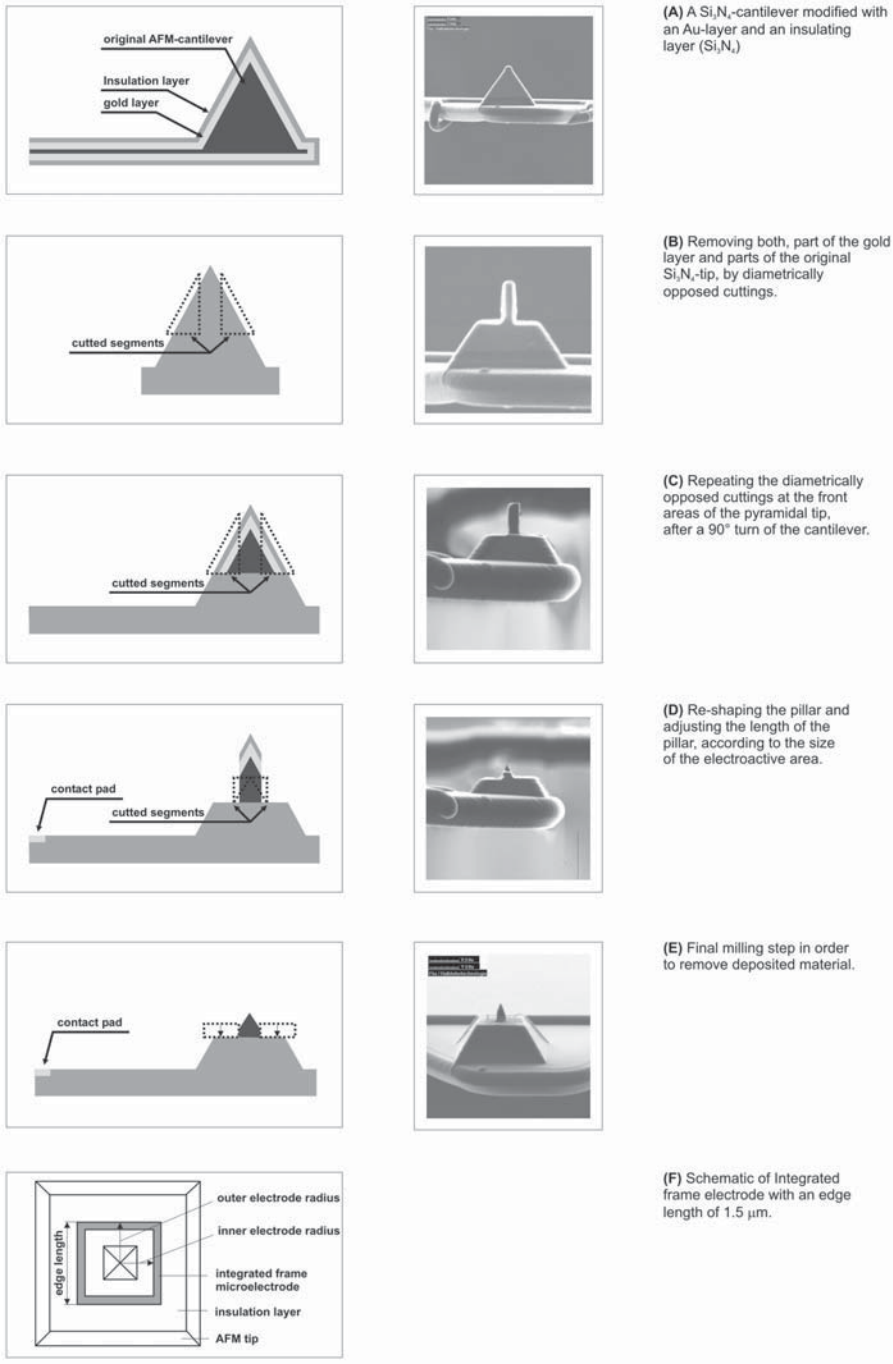

Fig. 1. **(A–F)** Modification steps of coated AFM tip using FIB technique showing (**left**) schematic view of processing step and (**right**) corresponding FIB images. (From **ref. *6*** with permission.)

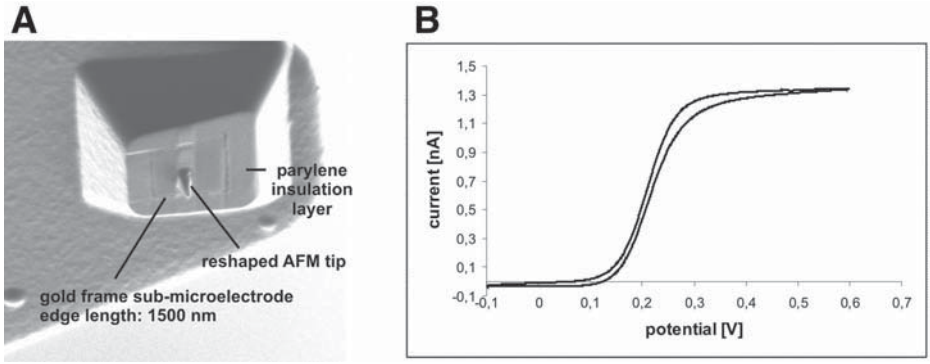

Fig. 2. **(A)** FIB images of integrated frame submicroelectrode with edge length of 1500 nm and tip height of 800 nm; **(B)** cyclic voltammogram recorded at this frame submicroelectrode for oxidation of 0.01 mol/L of $K_4[Fe(CN)_6]$ in 0.5 mol/L of KCl (scan rate: 100 mV/s).

and the sample surface within the working distance for electrochemical imaging of the surface properties.

3.1.3. Electrochemical Characterization of Tip-Integrated Frame Microelectrodes

Electrochemical characterization of the integrated microelectrodes was done by cyclic voltammetry using 0.01 mol/L of $K_4[Fe(CN)_6]$ in 0.5 mol/L of KCl as a supporting electrolyte (**Fig. 2B**). Currently, no theoretical description for square-frame electrode geometries is available in the literature. Development of a suitable theory is in progress. Hence, the theoretical description of ring microelectrodes was used for characterization of the electrochemical behavior. The steady-state current response of a ring microelectrode can be described using **Eqs. 1–3** ***(20,21)***:

$$I_d = nFDc^* l_0 \tag{1}$$

in which

$$l_0 = \frac{\pi^2(a+b)}{\ln[16(a+b)/(b-a)]} \tag{2}$$

for $a/b > 0.91$, and

$$l_0 = \frac{\pi^2(a+b)}{\ln[32a/(b-a) + \exp(\pi^2/4)]} \tag{3}$$

for all other ratios *a*/*b*. In **Eqs. 1–3**, *D* and c^* are the diffusion coefficient and the bulk concentration of the redox mediator, respectively; *F* is the Faraday constant; *n* is the number of transferred electrons; *a* is the inner electrode radius; and *b* is the outer electrode radius (*see* **Fig. 1F**). Based on **Eqs. 1** and **2**, the theoretical steady-state current for the oxidation of 0.01 mol/L of $[Fe(CN)_6]^{4-}$ with $n = 1$ for the cyclic voltammogram of the frame microelectrode shown in **Fig. 2A** (inner radius $a = 650$ nm; outer radius $b = 750$ nm; ratio $a/b = 0.867$) is calculated to be 1.65 nA (diffusion coefficient: 6.7×10^{-6} cm^2/s ***[4]***). The experimentally observed steady-state current is 1.4 nA. However, it has to be considered that the diffusion behavior towards a frame electrode differs from the ring geometry owing to additional effects occurring at the edges of the frame geometry.

3.2. Preparation of Sample

The simultaneous imaging of the topographical and electrochemical properties of a soft biological sample with bifunctional AFM-SECM probes is described. As a test sample, the pores of a periodic microstructure were filled with a soft polymer matrix entrapping the enzyme glucose oxidase ***(14)*** (*see* **Note 3**).

Figure 3 illustrates the fabrication steps of the sample surface along with AFM images. A periodically micropatterned silicon nitride layer (450-nm layer thickness) was deposited onto a gold-coated silicon wafer (*see* **Note 4**). The conductive gold layer was used as a working electrode to electrochemically deposit the glucose oxidase-containing polymer films based on pH shift–induced precipitation (**Fig. 3A,B**) ***(22)***. A solution containing glucose oxidase (5 mg/mL of water) and Canguard polymer suspension (70 µL/mL of water) was stored for at least 30 min at 4°C before it was used. A three-electrode setup was used with an oxidized silver wire operating as the AgQRef, a platinum wire as the auxiliary electrode, and the conductive gold layer of the micropattern as the working electrode. For polymer film formation with the enzyme present in solution, a potential-pulse profile (2200 mV for 0.2 s, 800 mV for 1 s, and 0 mV for 5 s vs AgQRef) was applied 12 times, leading to the precipitation of the polymer in the pores entrapping the enzyme. The sample was rinsed with water and phosphate buffer and stored for at least 12 h at 4°C before analysis with AFM-SECM.

3.3. Simultaneous Topographical and Electrochemical Imaging of Enzyme Activity

The experimental setup and the parameters for AFM-SECM imaging of enzyme activity are described in **Subheadings 3.3.1.–3.3.4.** This includes a description of the instrumentation, the parameters chosen for AFM tapping mode, and the parameters for simultaneous electrochemical imaging.

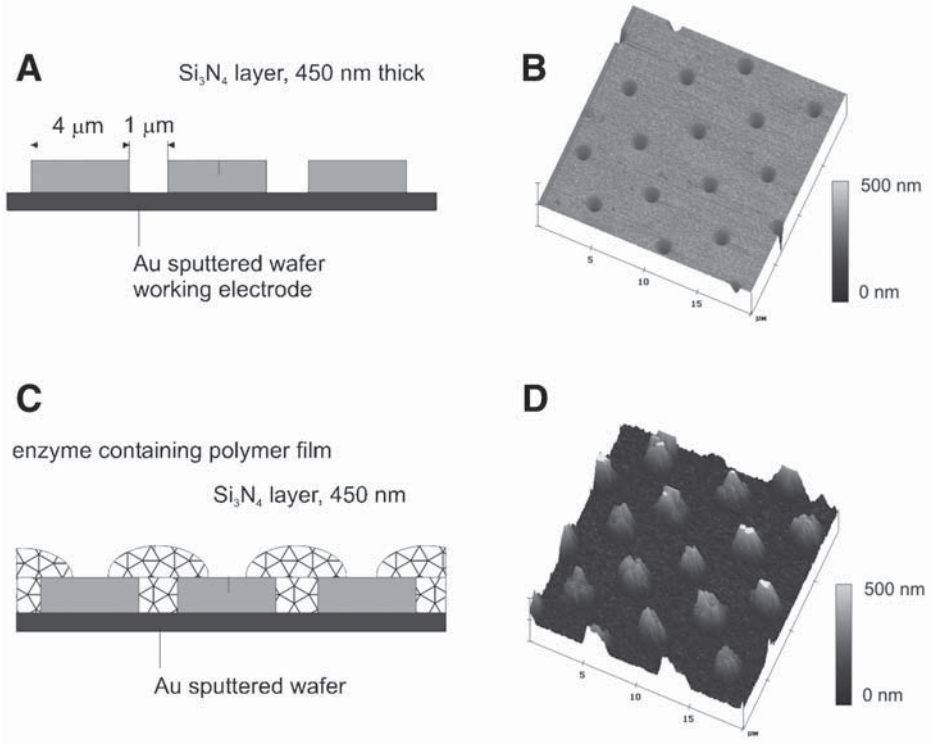

Fig. 3. Schematic view of sample and corresponding AFM contact mode images **(A,B)** before and **(C,D)** after precipitation of enzyme containing polymer film.

3.3.1. Instrumentation: Experimental Setup

The modified tip was mounted into a Nanoscope III, equipped with a tapping mode fluid cell using the liquid inlet and outlet for positioning a Pt wire as the counterelectrode and an oxidized Ag wire as the AgQRef. The electrical contact for the integrated electrode is provided by the gold spring holding the cantilever in the fluid cell. The spring is pressed onto a small exposed area of the gold layer at the end of the cantilever mount. The contact window was opened by mechanically scratching the insulation layer with a needle or tweezers with sharp, pointy ends. After contacting, the cantilever mount was protected by an insulation varnish applied with a fine microbrush.

An overview of the experimental setup is shown in **Fig. 4**. The electrochemical experiment is controlled with a bipotentiostat, and the electrochemical signal is read into an additional AD channel of the AFM instrument, which is provided by all conventional atomic force microscopes (*see* **Note 5**). Thus, the current measured with the integrated electrode can be directly correlated to the topographical information obtained by the reshaped AFM tip.

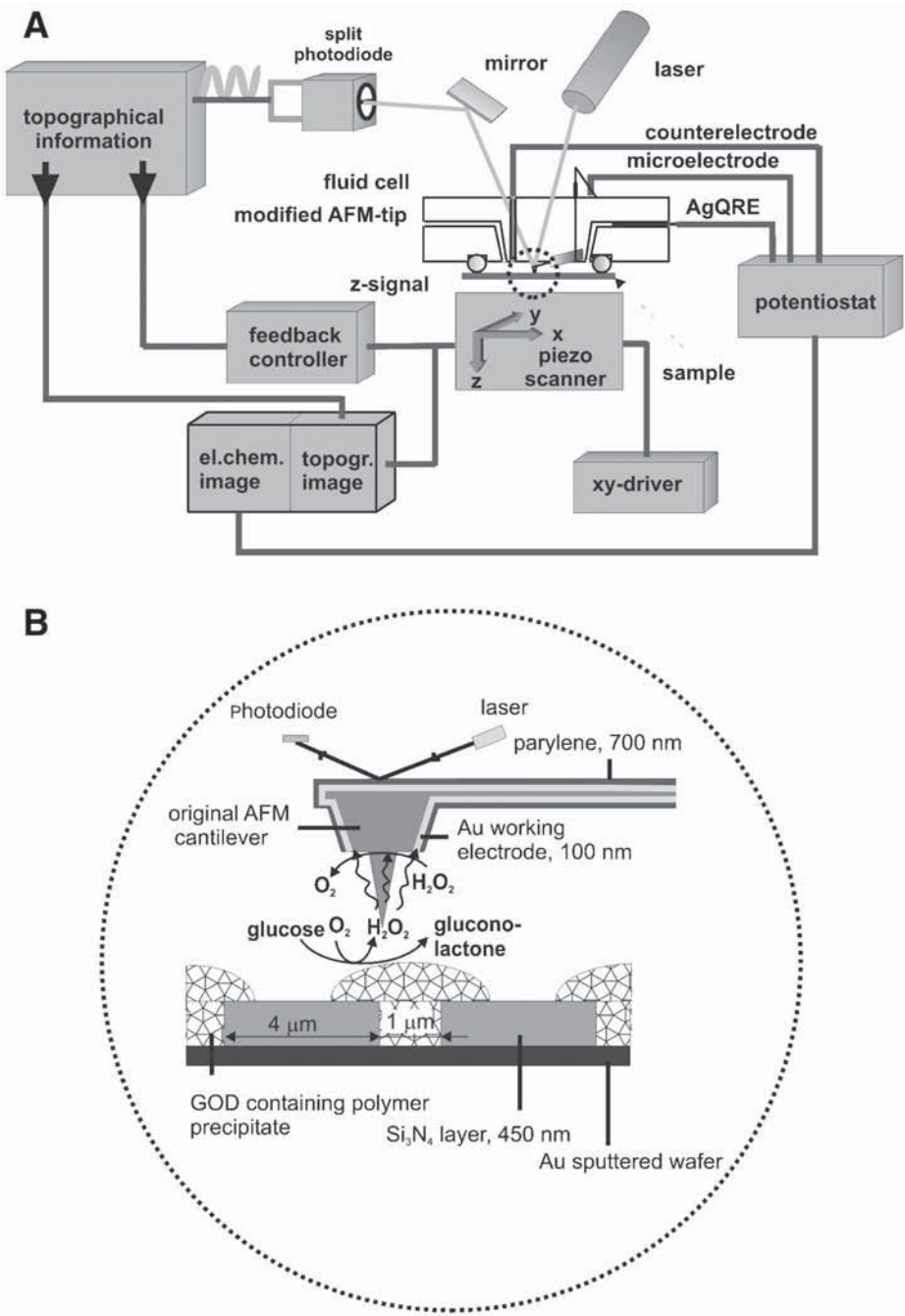

Fig. 4. **(A)** Experimental setup and **(B)** scheme of simultaneous AFM-SECM imaging and involved reactions at surface of micropatterned sample with integrated electrode operating in generation-collection mode.

3.3.2. Tapping Mode Imaging

For simultaneous topographical and electrochemical imaging of the enzyme activity, the integrated electrode is scanned over the sample surface in AFM tapping mode using the DI tapping mode liquid cell filled with air-saturated phosphate buffer. The parameters for AFM tapping mode imaging are as follows:

1. Drive frequency: 32.4 V (*see* **Note 6**).
2. Drive amplitude: 5 V (*see* **Note 7**).
3. Scan rate: 2 Hz (*see* **Note 8**).
4. Set point: 0.6 V (*see* **Note 9**).
5. Sampling rate: 256 × 256.

The integral gain and proportional gain should be optimized for every measurement so that the height image shows the sharpest contrast and there are minimal variations in the amplitude image (the error signal).

3.3.3. Electrochemical Imaging

For localized detection of glucose oxidase activity, the generation-collection mode of SECM ***(23)*** has been applied. In the presence of the substrate glucose, H_2O_2 is locally generated as a byproduct of the enzymatic reaction. Glucose oxidase catalyzes the oxidation of glucose to gluconolactone, and the electron acceptor oxygen of the enzymatic reaction is reduced to H_2O_2 (**Fig. 4B**). H_2O_2 is directly detected at the integrated electrode using amperometry at a constant applied potential of 750 mV vs AgQRef. A schematic of the involved reactions and the measurement principle is given in **Fig. 4B**.

The parameters for electrochemical imaging are as follows:

1. Technique: amperometry.
2. Counterelectrode: Pt wire.
3. Quasi-reference electrode: oxidized Ag wire.
4. Tip potential: 750 mV vs AgQRef.
5. Sample interval: 0.0025 s.
6. Liquid: for negative control, phosphate buffer (0.1 *M*, pH 7.0), air saturated; for positive control, add 50 m*M* glucose.

3.3.4. Simultaneous AFM-SECM Imaging

The tip was engaged to the surface and the image quality optimized (*see* **Subheading 3.3.1.**) showing the topographic features of the polymer spots. Subsequently, the potential was applied to the integrated electrode and the current was recorded as a negative control image (**Fig. 5A–C**). In the absence of glucose in solution, the current recorded at the electrode during AFM tapping mode imaging of the enzyme containing polymer spots was negligible and

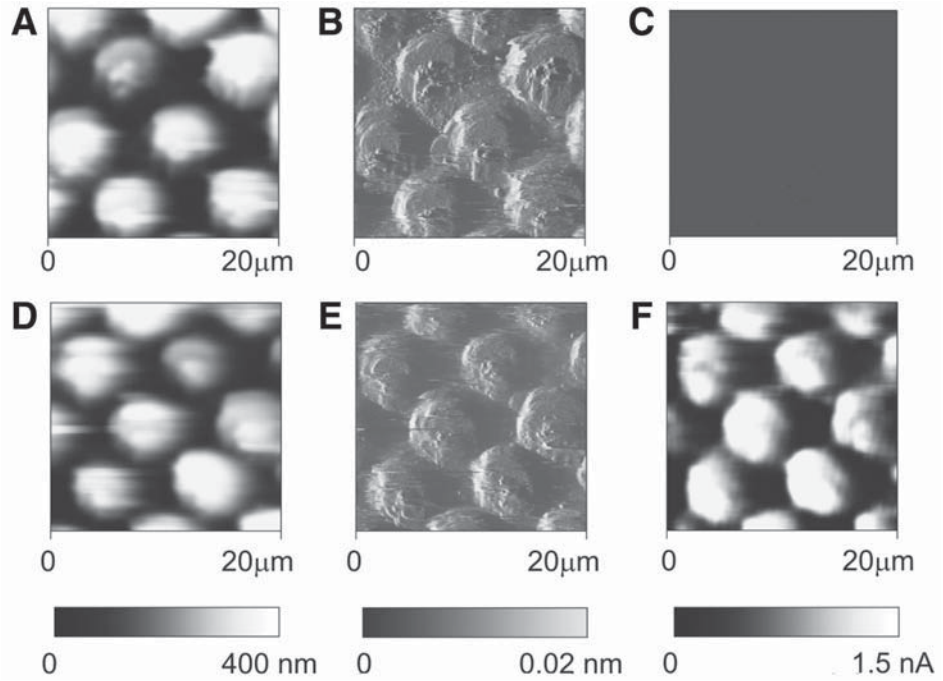

Fig. 5. Simultaneously recorded height and current images of glucose oxidase activity in AFM tapping mode with free-drive amplitude of 5 V and drive frequency of 32.4 kHz. Top view of the height **(A,D)**, corresponding amplitude **(B,E)**, and simultaneously recorded current **(C,F)** images recorded in air-saturated phosphate buffer (0.1 mol/L, pH 7.4) in the absence (A–C) and presence (D–F) (50 m*M*) of the substrate glucose in solution is shown. The tip was held at a potential of 750 mV vs AgQRef. Electrode edge length: 770 nm; tip height: 700 nm. (From **ref. *14*** with permission.)

revealed no electrochemical features (**Fig. 5C**). For mapping the enzyme activity, the tip was retracted and the fluid cell was filled with phosphate buffer containing 50 m*M* glucose. After reengagement of the tip, the scanning procedure was repeated. In the presence of glucose, an increase in the current recorded at the nanoelectrode was obtained owing to the localized production of H_2O_2 when the tip was scanned across the glucose oxidase containing polymer spots (**Fig. 5F**). The periodicity of the pattern in the electrochemical image corresponds well with the topography provided by the integrated AFM tip. Furthermore, the topography features in the negative and positive control are unaltered but do not give any information about the immobilized enzyme activity.

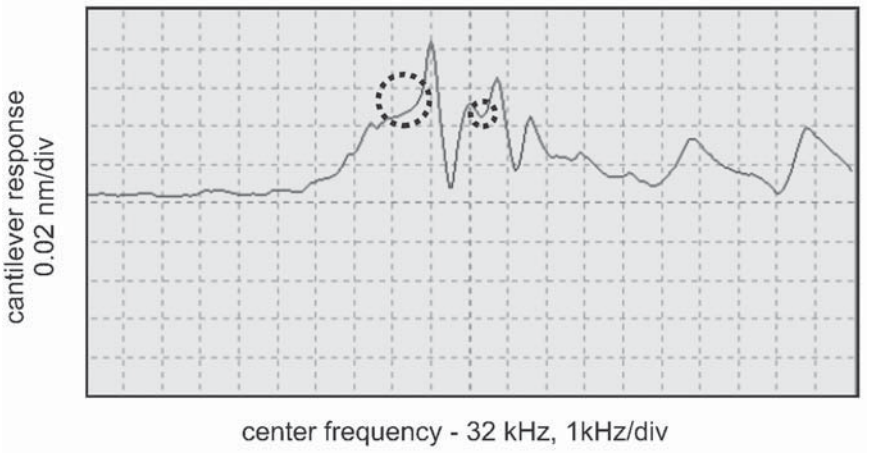

Fig. 6. Frequency spectrum of modified cantilever coated with 100 nm of Au and insulated with 700 nm of parylene C.

4. Notes

1. Alternatively, a 50-nm Pt layer can be deposited as an electrode material (working pressure: 6 mtorr; power: 30 W; under argon). Higher power results in bending of the cantilever.
2. The metallized cantilevers can also be insulated by applying an 800-nm-thick layer of silicon nitride deposited by PECVD. Dense and well-defined insulation layers are particularly achievable when the process is repeated several times (6 × 5 min PECVD deposition, resulting in approx 800 nm of Si_3N_4) ***(6)***.
3. The described immobilization protocol can be applied to a number of other proteins. For example, entrapment of catalase, lactate oxidase, pyrovate oxidase, NAD^+-dependent glucose dehydrogenase, pyrroloquinoline quinone (PQQ)-dependent glucose dehydrogenase, quinohemoprotein alcohol dehydrogenase, and alcohol dehydrogenase has been reported in the literature ***(22).***
4. The periodically micropatterned wafer was purchased from Quantifoil. Any microelectrode array can be used for this purpose.
5. Digital Instruments offers a phase box for reading in up to four additional signals.
6. Despite deposition of 100 nm of gold and 700 nm of parylene C, the properties of the initial silicon nitride cantilever remain virtually unaltered compared with unmodified Si_3N_4 cantilevers ***(9)***. Anyway, the optimal drive frequency varies for different samples, fluids, fluid volumes, and cantilevers, and, hence, the drive frequency has to be chosen manually following the DI operation instructions. The best frequencies appear to be on the side of a peak or in a shallow valley between peaks. A typical frequency spectrum of a modified cantilever is depicted in **Fig. 6**. The regions circled show typical operation frequencies that produce good fluid tapping images.

7. The drive amplitude is adjusted until the desired cantilever response amplitude is obtained. For samples with small variations in height, usually drive amplitudes of 2 to 5 V are required. Good results are usually not obtained on soft samples if it is necessary to use drive amplitudes above 10 V.
8. In general, low scan rates of 1 Hz or lower are advantageous in order to avoid convective effects.
9. The set point can be adjusted by monitoring the image quality. Increase the set point in small increments until the cantilever pulls off the surface. Then reduce the set point in small increments until an image appears and the image is optimized. Usually the best images are obtained at set points just below where an image appears.

Acknowledgments

This work was supported by the National Science Foundation (grant 0216368 within the program Biocomplexity in the Environment), the National Institute of Health (grant EB00058), and the Fonds zur Förderung der wissenschaftlichen Forschung Austria (grants P14122-CHE and J2230).

References

1 Binnig, G., Quate, C. F., and Gerber, C. (1986) Atomic force microscopy. *Phys. Rev. Lett.* **56,** 930–933.
2. Liu, H. Y., Fan, F.-R. F., Lin, C. W., and Bard, A. J. (1986) Scanning electrochemical and tunneling ultramicroelectrode microscope for high-resolution examination of electrode surfaces in solution. *J. Am. Chem. Soc.* **108,** 3838, 3839.
3. Engstrom, R. C., Weber, M., Wunder, D. J., Burgess, R., and Winquist, S. (1986) Measurements within the diffusion layer using a microelectrode probe. *Anal. Chem.* **58,** 844–848.
4. Kwak, J. and Bard, A. J. (1989) Scanning electrochemical microscopy: theory of the feedback mode. *Anal. Chem.* **61,** 1221–1227.
5 Gardner, C. E. and Macpherson, J. V. (2002) Atomic force microscopy probes go electrochemical. *Anal. Chem.* **74,** 576A–584A.
6 Kranz, C., Friedbacher, G., Mizaikoff, B., Lugstein, A., Smoliner, J., and Bertagnolli, E. (2001) Integrating an ultramicroelectrode in an AFM cantilever: combined technology for enhanced information. *Anal. Chem.* **73,** 2491–2500.
7. Krantz, C., Mizaikoff, B., Lugstein, A., and Bertagnolli, E. (2002) Integrating an ultramicroelectrode in an AFM cantileuer: toward the development of combined microsensing imaging tools: in Environmental Electrochemistry Analysis of Trace Element Biogeochemistry (Taillefert, M. and Rozan, T. F., eds.), American Chemical Society, Washington, DC, pp. 320–333.
8 Lugstein, A., Bertagnolli, E., Kranz, C., Kueng, A., and Mizaikoff, B. (2002) Integrating micro- and nanoelectrodes into atomic force microscopy cantilevers using focused ion beam techniques. *Appl. Phys. Lett.* **81,** 349–351.

9 Kueng, A., Kranz, C., Mizaikoff, B., Lugstein, A., and Bertagnolli, E. (2003) Combined scanning electrochemical atomic force microscopy for tapping mode imaging. *Appl. Phys. Lett.* **82,** 1592–1594.
10 Hansma, P. K., Cleveland, J. P., Radmacher, M., et al. (1994) Tapping mode atomic force microscopy in liquids. *Appl. Phys. Lett.* **64,** 1738–1740.
11 Putman, C. A. J., van der Werf, K. O., De Grooth, B. G., Van Hulst, N. F., and Greve, J. (1994) Tapping mode atomic force microscopy in liquid. *Appl. Phys. Lett.* **64,** 2454–2456.
12 Le Grimellec, C., Giocondi, M. C., Pujol, R., and Lesniewska, E. (2000) Tapping mode atomic force microscopy allows the in situ imaging of fragile membrane structures and of intact cell surfaces at high resolution. *Single Molecules* **1,** 105–107.
13. Knoll, A., Magerle, R., and Krausch, G. (2001) Tapping mode atomic force microscopy on polymers: where is the true sample surface? *Macromolecules* **34,** 4159–4165.
14 Kueng, A., Kranz, C., Lugstein, A., Bertagnolli, E., and Mizaikoff, B. (2003) Integrated AFM-SECM in tapping mode: simultaneous topographical and electrochemical imaging of enzyme activity. *Angew. Chem. Int. Ed.* **42,** 3237–3240.
15 Kueng, A., Kranz, C., and Mizaikoff, B. (2003) Scanning probe microscopy with integrated biosensors. *Sens. Lett.* **1,** 2–15.
16 Kueng, A., Kranz, C., and Mizaikoff, B. (2004) Amperometric ATP-biosensor based on polymer entrapped enzymes. *Biosens. Bioelectron.* **19,** 1301–1307.
17 Kranz, C., Kueng, A., Lugstein, A., Bertagnolli, E., and Mizaikoff, B. (2004) Mapping of enzyme activity by detection of enzymatic products during AFM imaging with integrated SECM-AFM probes. *Ultramicroscopy* **100,** 127–134.
18. Heintz, E. L. H., Kranz, C., Mizaikoff, B., Noh, H.-S., Hesketh, P., Lugstein, A., and Bertagnolli, E. (2001) Characterization of parylene coated combined scanning probe tips for in-situ electrochemical and topographical imaging, in *Proceedings of the IEEE Nanotechnology Conference*.
19 Lee, Y., Amemya, S., and Bard, A. J. (2001) Scanning electrochemical microscopy. 41. Theory and characterization of ring electrodes. *Anal. Chem.* **73,** 2261–2267.
20. Smythe, W. R. (1951) The capacitance of a circular annulus. *J. Appl. Phys.* **22,** 1499–1501.
21. Szabo, A. J. (1987) Theory of current at microelectrodes: application to ring electrodes. *J. Phys. Chem.* **91,** 3108–3111.
22 Kurzawa, C., Hengstenberg, A., and Schuhmann, W. (2002) Immobilization method for the preparation of biosensors based on pH shift-induced deposition of biomolecule-containing polymer films. *Anal. Chem.* **74,** 355–361.
23. Wittstock, G. (2001) Modification and characterization of artificially patterned enzymatically active surfaces by scanning electrochemical microscopy. *Fresenius J. Anal. Chem.* **370,** 303–315.